Enhanced lipogenesis through Ppar γ helps cavefish adapt to food scarcity

Highlights

- Cavefish store large amounts of fat when fed ad libitum in the lab
- Cavefish show an improved ability to use lipogenesis to convert energy into fat
- The lipid metabolism regulator Ppar γ is upregulated in cavefish livers
- Cavefish carry a nonsense mutation in per2, a known repressor of Pparγ

Authors

Shaolei Xiong, Wei Wang, Alexander Kenzior, ..., John M. Miles, Alejandro Sánchez Alvarado, Nicolas Rohner

Correspondence

nro@stowers.org

In brief

Cavefish have evolved an impressive ability to store fat during times of plenty to survive long periods of starvation. On a cellular level, this is due to an increased ability to convert available energy into fat through lipogenesis.









Report

Enhanced lipogenesis through Ppary helps cavefish adapt to food scarcity

Shaolei Xiong, Wei Wang, 1,2,3 Alexander Kenzior, Luke Olsen, 1,4 Jaya Krishnan, Jenna Persons, Kyle Medley, 1 Robert Peuß, 1,5 Yongfu Wang, 1 Shiyuan Chen, 1 Ning Zhang, 1 Nancy Thomas, 1 John M. Miles, 6

Alejandro Sánchez Alvarado, 1,2 and Nicolas Rohner 1,4,7,8,*

⁷Twitter: @NicolasRohner

⁸Lead contact

*Correspondence: nro@stowers.org https://doi.org/10.1016/j.cub.2022.03.038

SUMMARY

Nutrient availability varies seasonally and spatially in the wild. While many animals, such as hibernating animals or migrating birds, evolved strategies to overcome periods of nutrient scarcity, 1,2 the cellular mechanisms of these strategies are poorly understood. Cave environments represent an example of nutrientdeprived environments, since the lack of sunlight and therefore primary energy production drastically diminishes the nutrient availability.³ Here, we used *Astyanax mexicanus*, which includes river-dwelling surface fish and cave-adapted cavefish populations, to study the genetic adaptation to nutrient limitations. 4-9 We show that cavefish populations store large amounts of fat in different body regions when fed ad libitum in the lab. We found higher expression of lipogenesis genes in cavefish livers when fed the same amount of food as surface fish, suggesting an improved ability of cavefish to use lipogenesis to convert available energy into triglycerides for storage into adipose tissue. 10-12 Moreover, the lipid metabolism regulator, peroxisome proliferator-activated receptor γ (Ppar γ), is upregulated at both transcript and protein levels in cavefish livers. Chromatin immunoprecipitation sequencing (ChIP-seg) showed that Ppar γ binds cavefish promoter regions of genes to a higher extent than surface fish and inhibiting Ppary in vivo decreases fat accumulation in A. mexicanus. Finally, we identified nonsense mutations in per2, a known repressor of Ppary, providing a possible regulatory mechanism of Ppary in cavefish. Taken together, our study reveals that upregulated Ppar γ promotes higher levels of lipogenesis in the liver and contributes to higher body fat accumulation in cavefish populations, an important adaptation to nutrient-limited environments.

RESULTS

Cavefish display increased body fat levels throughout

Previous studies have shown that compared to surface fish, cavefish populations display higher total triglycerides and visceral fat when fed ad libitum.4-6 To confirm these findings and develop a method to more easily quantify total body fat in fish, we used EchoMRI to measure body fat percentage. Consistent with previous total triglycerides measurements, 4 fish from both the Pachón and Tinaja populations showed higher body fat than surface fish (median surface = 15.2%; median Pachón = 33.4%; median Tinaja = 29.4%; Figure 1A). To better visualize fat distribution throughout the body, we dissected adult fish into various sections and used hematoxylin and eosin (H&E) staining of head and trunk sections. We observed that Tinaja and Pachón cavefish store fat in the entire eye socket, which is nearly absent in surface fish (Figures 1B and S1A-S1C). Tinaja and Pachón cavefish have markedly more adipocytes in the ventral part and lateral sides of the trunk compared to surface fish (Figures 1C and S1A). In the dorsal part of the trunk, we observed only slightly more adipocytes in cavefish as compared to surface fish (Figure 1C). In total, the relative adipose area in the transverse trunk section of cavefish was significantly higher than that of surface fish (Figure 1D). Additionally, we used the Folch method, which takes advantage of the biphasic solvent system consisting of chloroform/methanol/water¹³ to extract and guantify total lipid content from head, dorsal, and ventral parts of the trunk (Figure 1E). We found Tinaja and Pachón cavefish have a higher lipid content in the head, dorsal trunk, and ventral trunk sections compared to surface fish (Figure 1E). Notably, we found no difference in hepatic triglyceride and total liver lipid between



¹Stowers Institute for Medical Research, Kansas City, MO 64110, USA

²Howard Hughes Medical Institute, Kansas City, MO 64110, USA

³National Institute of Biological Sciences, Beijing 102206, China

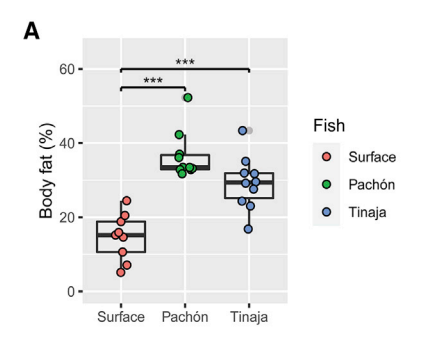
⁴Department of Molecular & Integrative Physiology, University of Kansas Medical Center, Kansas City, KS 66160, USA

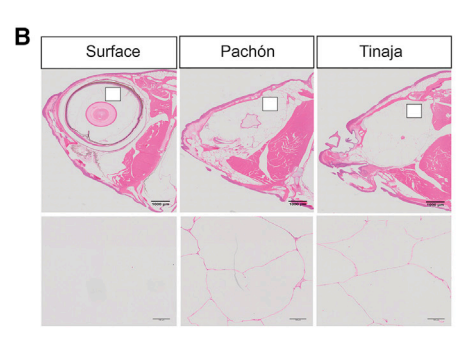
⁵Institute for Evolution and Biodiversity, University of Münster, Münster 48149, Germany

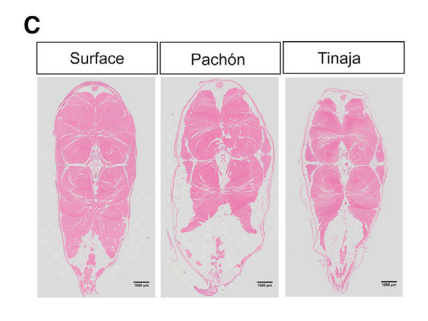
Department of Medicine, Division of Metabolism, Endocrinology & Genetics, University of Kansas Medical Center, Kansas City, KS 66160,

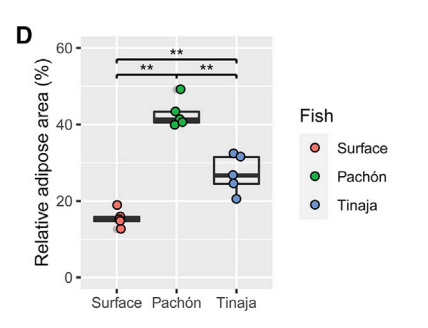
Report

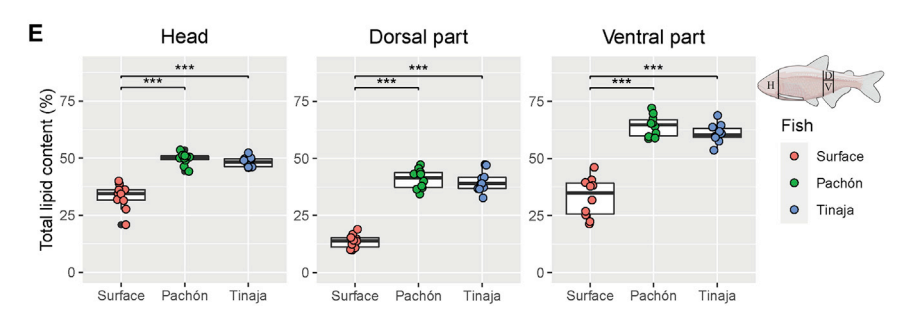












adult surface fish and cavefish populations (Figures S1D and S1E), indicating that 1-year-old cavefish do not over-accumulate lipids in the liver, at least on our lab feeding regime (see STAR Methods for detail).

Cavefish have increased lipogenesis in the liver

Given the differences in body fat content between cavefish and surface fish populations throughout different body parts, we hypothesized that cavefish display higher postprandial lipid anabolism than surface fish. This should be particularly pronounced in Pachón cavefish as they are known to have similar appetites as surface fish.^{4,7} To study the transcriptional response to feeding, we first fasted juvenile Pachón cavefish and surface fish for 4 days to allow transcription of anabolic genes to reduce to similar levels between the two fish populations. We then refed the different populations the same amount of food (10 mg), collected liver samples 3 h after refeeding, and performed bulk RNA sequencing (RNA-seg) of liver tissue, which is a primary center of lipogenesis (Figure 2A). We identified ~16,000 genes (transcript per million [TPM] > 1), of which \sim 2,300 were differentially expressed (DE) between the refed Pachón and surface fish samples (Figures S2A and S2B; Table S1). We performed Gene Ontology

Figure 1. Cavefish display more body fat in various areas of the body compared to surface fish

(A) Total body fat comparison (fat mass/total body weight) between adult (1-year-old) surface fish, and Pachón and Tinaja cavefish using EchoMRI (n = 9, 10, 10, respectively).

(B) H&E staining of fish head sections of the three fish populations (Surface, Pachón, and Tinaja). The sagittal sections were performed across the eye area of the head, the upper panel showing the entire section and the lower panel showing the region indicated with a white box in the upper panel, revealing that the orbit (eye socket) in cave-fish is filled with adipocytes (n = 5 per population; scale bar: 1 mm in the upper panel; scale bar: 100 μm in the bottom panel).

(C) Transverse H&E staining of fish trunk sections close to the anal fin of the three fish populations (n = 5 per population; scale bar: 1 mm).

(D) Quantification of fat area to the whole transverse trunk section area in surface fish, Pachón, and Tinaja cavefish using "convert to mask" in ImageJ (n = 5 per population).

(E) Total lipid content (%) in surface fish, Pachón, and Tinaja cavefish (n = 10 per population) using the Folch method. Cartoon highlighting sampling areas for total lipid content quantification (H, head; D, dorsal part; V, ventral part; black lines indicate the boundaries of sampling). Significances calculated with Wilcoxon test, **p < 0.01.

(GO)-term enrichment analysis of the DE genes and identified numerous overrepresented metabolic pathways in the cavefish samples (Figure 2B). Among these enriched terms in the cavefish samples, we identified lipid anabolic pathways such as fatty acid biosynthesis and triglyceride bio-

synthesis (Figure 2B). To further dissect these pathways, we focused our analyses on key genes of these pathways (i.e., aclya, acaca, fasn, scd, elovl6, gpam, dgat1b, dgat2, lpin1, acsl4a, oxsm, and olah) (Figure 2C). Interestingly, these genes showed similar expression level at the fasted state between surface fish and Pachón cavefish but much higher expression levels in refed Pachón cavefish compared to refed surface fish (Figure 2C). These results indicate a likely enhanced postprandial lipogenic capacity within the Pachón cavefish. We confirmed these results by focusing on three key fatty acid biosynthesis genes (ATP citrate lyase [acly], acetyl-CoA carboxylase 1 [acaca], and fatty acid synthase [fasn]) using qRT-PCR. All three genes responded to feeding by a 10-100 fold increased expression in Pachón cavefish compared to surface fish (Figure 2D), suggesting that Pachón cavefish have a greater ability to synthesize fatty acids following feeding than surface fish. Notably, we found a similar increase in expression of these genes in Tinaja and Molino cavefish populations (Figures S2C and S2D), indicating that enhanced lipogenesis capability is a common strategy in independently derived cavefish populations.

To better understand the temporal dynamics of postprandial gene expression, specifically the duration of increased



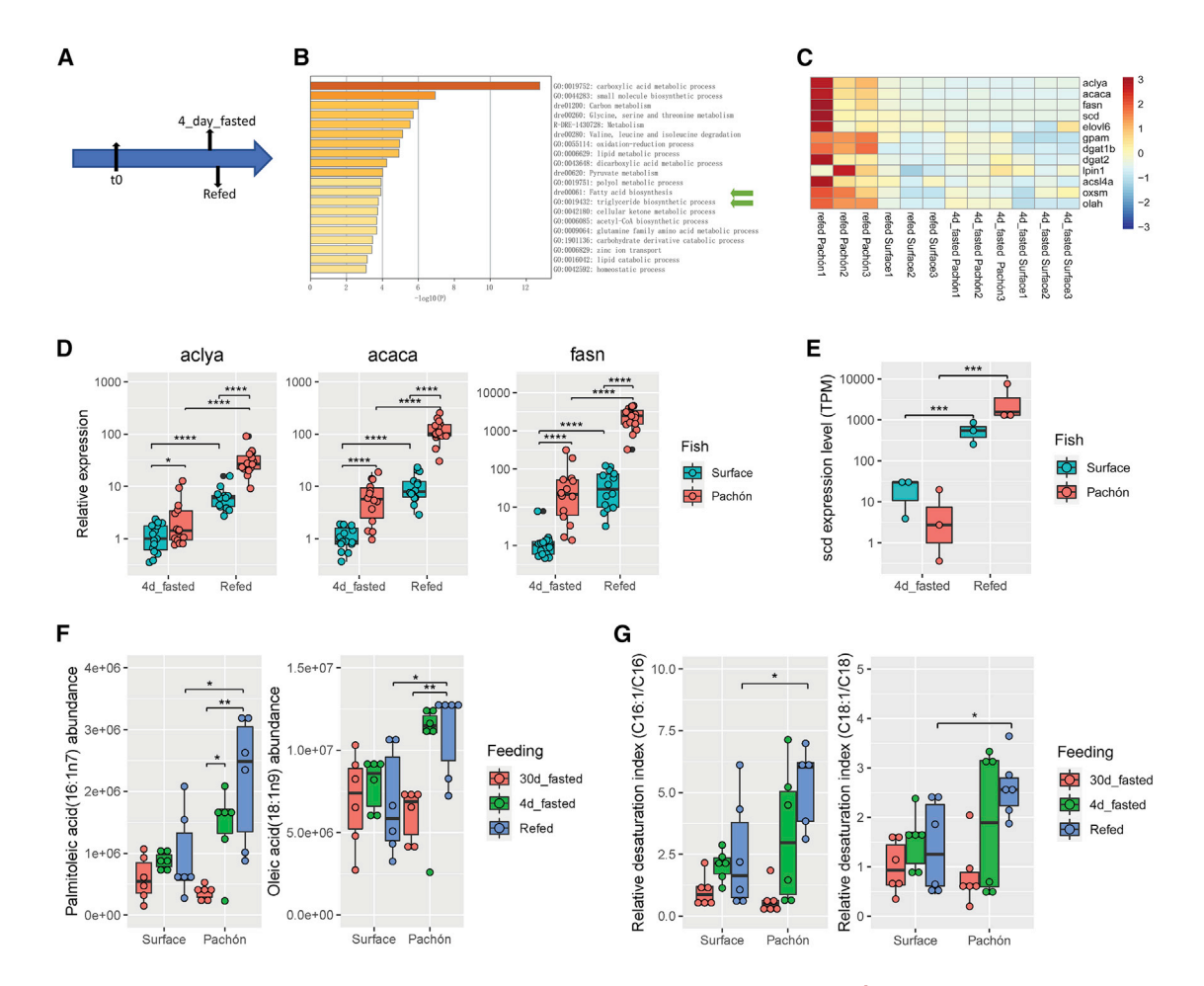


Figure 2. Lipogenesis genes are upregulated, and fatty acid profile is altered in the liver of Pachón cavefish compared to surface fish

- (A) Experimental design schematic for RNA-seq analysis of sub-adult (4 months) Pachón and surface fish (n = 3 per population and condition).
- (B) GO-term comparison and analysis of upregulated genes in refed Pachón and surface fish livers. Green arrows indicate the key lipid anabolic pathways, fatty acid biosynthesis, and triglyceride biosynthesis process.
- (C) Heatmap of lipogenesis genes in fasted and refed surface fish and Pachón cavefish.
- (D) Relative expression (RT-qPCR) of fatty acid biosynthesis genes in livers of 4-day fasted and refed surface fish and Pachón cavefish (n = 14 or 15; Wilcoxon test)
- (E) Expression of scd in livers of 4-day fasted and refed surface fish and Pachón cavefish (n = 3). TPM, transcript per million.
- (F) Fatty acid profiles of two MUFAs (n = 6 Wilcoxon test) data from Medley et al. 14
- (G) Refed Pachón cavefish livers have a higher desaturation index (C16:1n7/C16 and C18:1n9/C18) than surface fish (n = 6; Wilcoxon test) data from Medley et al. 14 *p < 0.05; **p < 0.01; ***p < 0.001.

lipogenesis, we performed a time course study of lipogenic gene expression. We measured transcription levels of key fatty acid biosynthesis genes (acly, acaca, and fasn) and triglyceride biosynthesis genes (scd1, elovl6, gpam, and dgat2) using qRT-PCR of liver tissues of surface fish and Pachón cavefish at different time points after paired feeding. We found higher expression of these lipogenesis genes in Pachón cavefish samples compared to surface fish up to 24 h after feeding, with the highest expression at the 6 h time point (Figure S2E). The gene expression differences were no longer detected at the 5-day time point. This indicates that upregulation of lipogenesis can last more than 24 h (but less than 5 days) after feeding the same amount of food in Pachón cavefish compared to surface fish.

To independently confirm whether increased lipogenesis in cavefish was occurring, we measured the products of fatty

acid desaturation, which are crucial for the generation of triglycerides from fatty acids. 11,15 The products of such conversion are monounsaturated fatty acids (MUFAs), chiefly oleate (18:1) and palmitoleate (c16:1). 16,17 Because this reaction is catalyzed by the scd gene product stearoyl-CoA desaturase, the expression level of scd gene and MUFA content reflect levels of active lipogenesis. We found mRNA expression of scd to be enhanced in Pachón cavefish liver samples compared to surface fish after feeding (Figure 2E). Using available lipidomics data, 14 we compared the abundance of MUFAs between surface fish and Pachón cavefish. We found that both oleic acid and palmitoleic acid were present in higher levels in refed Pachón cavefish livers compared to surface fish samples and cavefish samples starved for 30 days (Figure 2F). A further indicator of lipogenesis is the fatty acid desaturation index, the ratio of product (16:1n-7 and 18:1n-9) to precursor (16:0 and 18:0) fatty acids. 18-20 Indeed,

Report



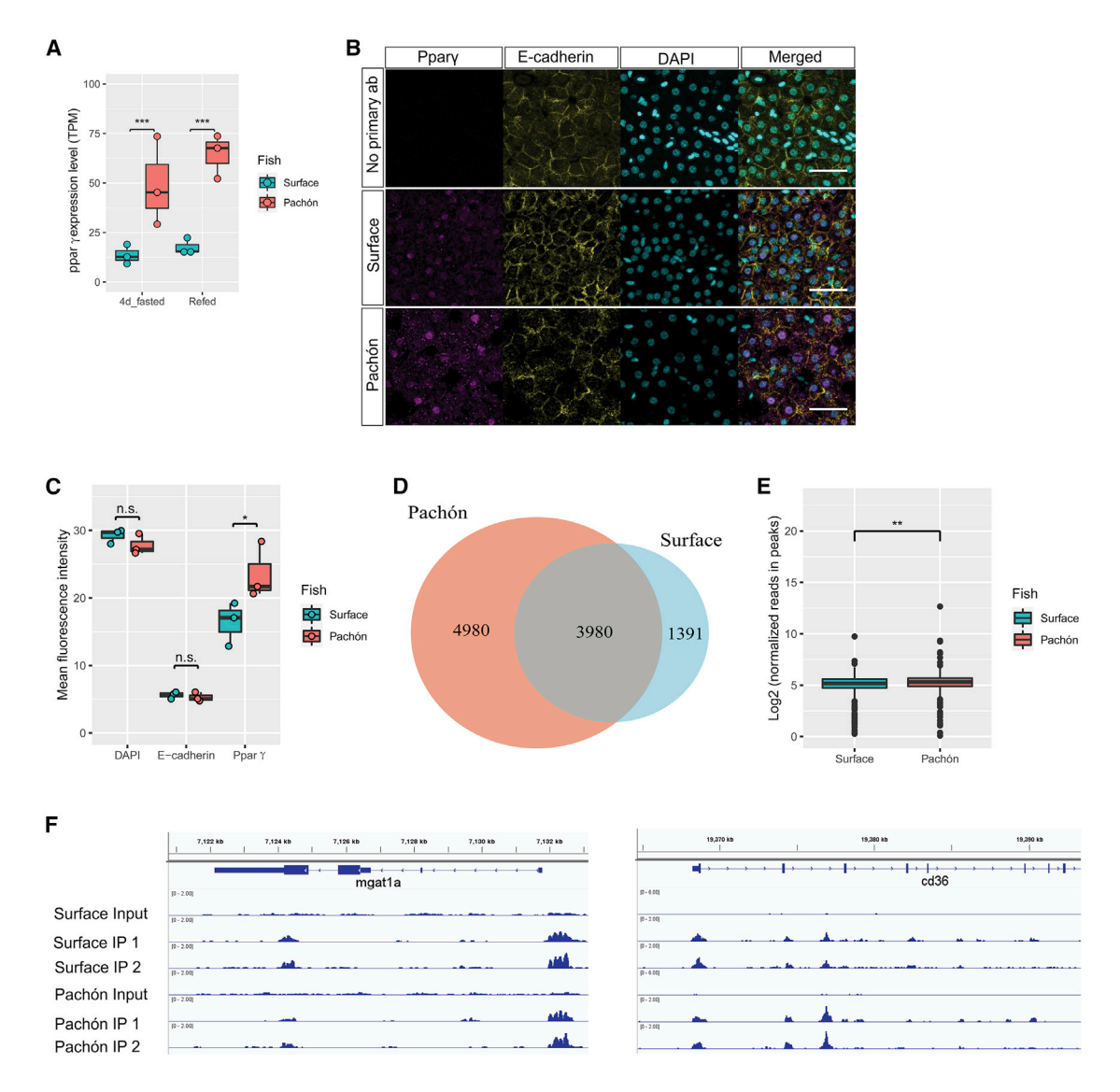


Figure 3. $ppar\gamma$ transcripts and Ppar γ protein is upregulated in cavefish livers

(A) pparγ mRNA expression level comparison between surface fish and Pachón cavefish under two feeding conditions: 4-day fasted and refed. TPM indicates transcript per million reads (n = 3 for each group, ***p < 0.001).

- (B) Immunostaining of Ppary (magenta), E-cadherin (yellow), and DAPI (turquoise) in liver sections of surface fish and Pachón cavefish. No primary ab, no primary antibody control. Scale bar: 30 µm.
- (C) Quantification of mean fluorescent intensity of Ppary staining (n = 3 for surface fish and Pachón livers. 187–317 hepatocytes were randomly selected from each fish liver sample for intensity measurement (Wilcoxon test, *p < 0.05).
- (D) Venn diagram of Pparγ ChIP-seq peaks within 3 kb of predicted transcription start sites in surface and Pachón cavefish livers.
- (E) Comparison of Ppary ChIP-seq peak height (in log2 normalized read number) between surface fish and Pachón cavefish (576 peaks with Ppary canonical binding sites. Wilcoxon test, **p < 0.01).
- (F) Examples of Ppary ChIP-seq peaks on known lipogenesis target genes (mgat1a or cd36).

we found that refed Pachón cavefish have a higher desaturation index for palmitoleic acid and oleic acid than surface fish (Figure 2G). Taken together, these data strongly suggest that Pachón cavefish have enhanced lipogenesis in the liver.

Ppar γ is upregulated in cavefish

We checked the expression of transcription factors known to regulate lipogenesis to identify whether these may be involved in the upregulation of lipogenesis gene expression observed in cavefish. We found no significant difference in expression of the genes coding for the transcription factors Srebp1, Chrebp, Lxr, and Usf (Usf1 and Usf2) between the surface and Pachón samples (Figure S2F). However, we noticed the gene peroxisome proliferator-activated receptor γ (ppar γ), encoding a transcription factor known to be a key regulator of adipogenesis and lipogenesis, 21-25 was significantly upregulated in Pachón cavefish samples at both the fasted and the refed state (Figure 3A). To test whether the differences in gene expression translate to



the protein level, we generated an antibody against Pparγ. To determine its specificity, we co-transfected either surface fish or Pachón cavefish pparγ along with GFP in HEK293T cell lines and immunostained the cells. Given that there are three amino acid differences between surface fish and Pachón cavefish Ppar γ , we performed the experiment with both sequences. Pparγ antibody localized only in the nuclei of cells that were positive for GFP as the transfection control, suggesting specificity of the antibody (Figure S3A). We next used the antibody to quantify Ppary protein levels in Astyanax mexicanus. We found slightly but significantly higher levels of Pparγ in the liver of Pachón cavefish compared to surface fish (Figures S3C and S3D). To visualize cellular distribution of Ppary, we performed immunofluorescence staining on liver sections. We found that Ppar γ was mainly expressed in the nucleus and again found visibly higher levels in Pachón cavefish hepatocytes compared to surface fish liver cells (Figures 3B and 3C). Furthermore, we did not detect Ppary antibody staining in the nucleus of blood cells within the liver tissue (Figure S3B). Given that Ppar γ is not known to be expressed in blood cells, this further argues for the specificity of the antibody. Together, these results show that Ppar γ is upregulated at the mRNA and protein levels in the liver of Pachón cavefish compared to surface fish.

To characterize whether increased protein levels translate into higher binding at the DNA level, we performed chromatin immunoprecipitation sequencing (ChIP-seq) for Pparγ in two livers of surface fish and Pachón cavefish. Pearson correlations between all samples showed high correlation between the biological replicates (Figure S4A). We used irreproducible discovery rate (IDR) to keep peaks that occurred consistently in both replicates and identified 5,371 high-confidence peaks (q value ≤ 0.01) located within 3 kb of the predicted transcription start sites for the surface fish samples and 8,960 peaks for the Pachón cavefish samples (Figures 3D and S4). 3,980 of those peaks were shared between two fish populations (Figure 3D). Since Ppary usually forms a heterodimer with Rxra, we searched all 10,251 peaks for the presence of the mouse Pparγ::Rxra motif using a Find Individual Motif Occurences scan to test if these peaks contain an enrichment for predicted Ppary binding sites. We identified the predicted mouse Pparγ::Rxra motif in 576 (5.56%) peaks, compared to a maximum of 268 (2.59%) motifs when randomly placing the same peaks in the transcription start site regions of all protein coding genes (repeated 1,000 times), suggesting an enrichment of potential Ppary binding sites in our dataset (Fisher's exact test, p < 1e-16; Table S2). In addition to more genomic binding in Pachón liver samples, we found these 576 peaks to be higher with significantly more reads than in the surface fish samples (Figure 3E). Notably, we identified genomic binding in known Ppary target genes involved in lipogenesis (e.g., mgat1a or cd36; Figure 3F). 23,26,27 These results are in line with our findings of higher levels of Pparγ in Pachón liver cells potentially driving expression of Ppary target genes to a higher extent than in surface fish liver cells, providing an important dataset of Ppary genome binding sites for future studies.

We next performed pharmacological experiments to test whether upregulation of $ppar\gamma$ in cavefish contributes to higher fat accumulation compared to surface fish. GW 9662 is a potent and selective Ppar γ antagonist, which has been used in human cell lines to inhibit Ppar γ . Consistent with the positive

correlation between $ppar\gamma$ expression level and body fat level, administration of 40 μM GW 9662 slowed down the fat accumulation in both fish populations at larvae stage (surface fish median size from 4000 μm^2 to 2000 μm^2 ; Pachón cavefish median size from 28000 μm^2 to 18000 μm^2), indicating $ppar\gamma$ promotes fat accumulation in Astyanax (Figures 4A and 4B). Notably, it delayed the onset of adipogenesis only in surface fish, but not in Pachón cavefish (Figure 4C). Specifically, the adipogenesis onset in surface fish dropped from 45.65% to 12.33% while it only reduced from 100% to 97.83% in Pachón cavefish. These results indicate that surface fish are more sensitive to Ppar γ inhibition than Pachón cavefish, probably because cavefish have elevated $ppar\gamma$ expression levels.

Nonsense mutations in the Ppary suppressor per2

Interestingly, we identified a genomic mutation in a known suppressor of Pparγ. Previously, it has been reported that period circadian clock 2 (Per2) suppresses Pparγ-mediated transcription by direct binding to its C-terminal domain.³⁰ Analyzing the RNA-seg data, we found that in Pachón liver samples, the per2 transcript is alternatively spliced, leading to a skipping of Exon 21 (Figure 4D). The final transcript contains a premature stop codon in Exon 22, which is predicted to lead to a truncation of 160 amino acids from Per2 C terminus in close proximity to the predicted Ppary binding domain (Figure 4D). We validated the splice variant using Sanger sequencing from cDNA generated from fresh fin, liver, brain, adipose, heart, and muscle tissue and found the alternatively spliced transcript to make up the majority, if not all, of the cDNA molecules (Figure 4E). We also found the same splice variant to be the predominant variant in samples of Tinaja cavefish, but not in Molino cavefish (Figures 4D and 4E). When we sequenced the Molino per2 transcript, we identified a different nonsense mutation further upstream of the Pachón and Tinaja variant. Molino cavefish carry a 7 basepair (bp) insertion in Exon 13 of per2, leading to a premature stop codon in Exon 13 and a loss of 855 amino acids from Per2, including the entire predicted Pparγ binding domain (Figure 4D). Notably, the 7 bp insertion also exists in wild-caught samples.31 The presence of two different nonsense mutations in per2 in three independently derived cavefish populations may imply loss-of-function mutations of per2 in cavefish and a putative role in cave adaptation. Interestingly, in the Somalian cavefish Phreatichthys andruzzi, per2 is found to have a nonsense mutation similar to the mutations we found in A. mexicanus (Figure 4D).³² A similar mutation in the same gene in a distantly related case of cave adaptation is an important example of convergent evolution of this gene in cave adaptation.

DISCUSSION

We sought to interrogate the cellular mechanisms contributing to high body fat accumulation in cavefish. First, we confirmed previous results showing that cavefish populations can store more fat than surface fish. Our study extends previous analyses by showing that cavefish store body fat in a variety of tissues and locations in the body with certain areas more prone to body fat storage than others. For example, our study did not find cavefish to develop a fatty liver, which is in contrast to previous findings. This can either be due to differences in the diet of



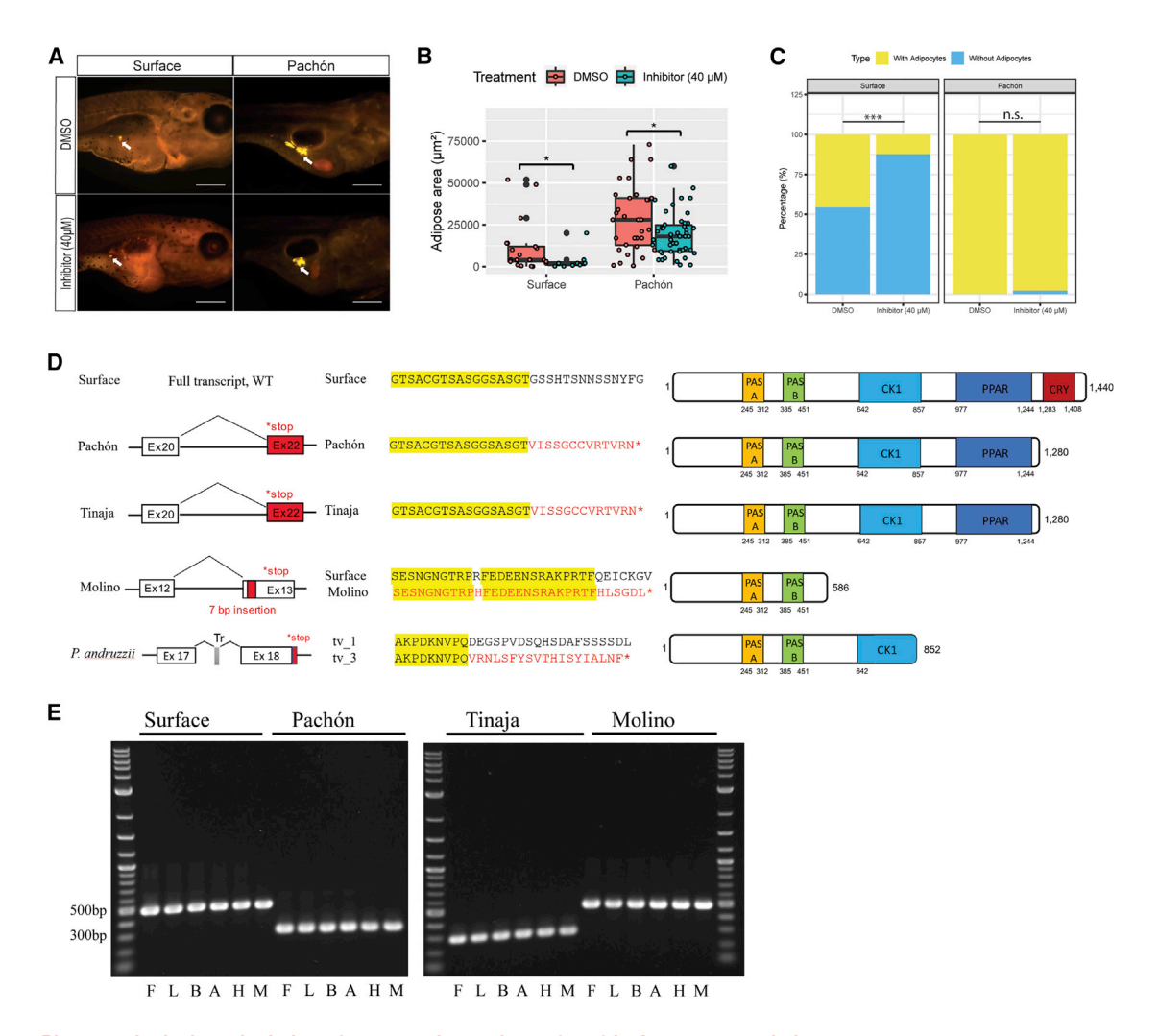


Figure 4. Pharmacological manipulation of $ppar\gamma$ and mutations of per2 in Astyanax populations

(A) Representative images of Nile red staining of surface fish and Pachón cavefish at 11 days post fertilization (dpf) raised under control conditions (0.2% dimethylsulfoxide [DMSO]) and PPARγ inhibitor, GW9662 (40 μM). Arrows indicate the locations of adipose tissue. Scale bar: 500 μm.

(B) Adipose tissue area comparison between surface fish and Pachón cavefish at 11 dpf raised under control condition and Ppar γ inhibitor (n = 21, 9, 32, 45 from left to right). Significance was calculated with Wilcoxon test: *p < 0.05.

(C) Comparison of the onset of adipogenesis between surface fish and Pachón cavefish at 11 dpf raised under control conditions and Ppar γ inhibitor (n = 46 surface DMSO; n = 73 surface inhibitor treatment; n = 32 Pachón DMSO; n = 46 Pachón inhibitor treatment). Significance was calculated with chi-square test: not significant (n.s.) p > 0.05; ***p < 0.001.

(D) Schematic depiction of the splice variant of *per2* leading to a skipping of Exon 21 and a premature stop codon in Exon 22 in Pachón and Tinaja cavefish. The 7 bp nucleotide insertion in Molino *per2* Exon 13 also leads to a premature stop codon. The dominant transcript of *per2* in *Phreatichthys andruzzii* (Somalian cavefish) carries a premature stop codon in Exon 18. The filled dark gray box (Tr), representing 225 bp nucleotides, shows the location of a transposon-derived sequence, which incorporated into the transcript leading to a premature stop codon. The middle panel shows the amino acid sequences near the stop codon. (tv_1: transcript variant 1; tv_3: transcript variant 3, which is the most abundant transcript). Right: schematic graphic of Per2 in Mexican cavefish and Somalian cavefish. PPAR, homology to predicted Pparγ binding domain; CRY, homology to Cry1 interacting region; PAS, homology to Per-Arnt-Sim domain; CK1, homology to casein kinase binding domain. Numbers indicate the amino acid number from N terminus (left) to C terminus (right).

(E) Gel images of per2 cDNA amplification in various tissues of Astyanax populations (F, fin; L, liver; B, brain; A, adipose tissue; H, heart; M, muscle).

the fish used for our study or the age of the fish used. We analyzed relatively young adult fish (\sim 1 year), while previous studies have used older fish. Studying the effect of factors including age and diets could further provide important insights into how cavefish can deal with the accumulation of liver fat, which causes nonalcoholic fatty liver disease in humans. ^{33,34} Furthermore, we developed a fast, reliable, and cheap method of quantifying total body fat in cavefish using EchoMRI, which

will open the door for high-throughput genetic analysis (i.e., quantitative trait loci analysis) of fat accumulation in future studies.

Using transcriptomic analysis, we uncovered a substantial upregulation of lipogenesis enzyme genes in the liver of Pachón cavefish compared to surface fish. Moreover, the lipidomic profiling demonstrated enhanced lipogenesis level in the Pachón cavefish. In comparison to surface fish, both of these lines of



evidence argue for an increased ability of cavefish to synthesize triglycerides either through de novo lipogenesis or breakdown of dietary fat. The food consumed by fish in our lab is protein rich (\sim 60%), arguing for a high turnover through de novo lipogenesis, which is in line with the observed upregulation of genes involved in fatty acid synthesis (acly, acaca, and fasn). However, the food also contains appreciable levels of fat (\sim 15%), which makes it likely that some of the triglyceride biosynthesis occurs through absorption and esterification of fatty acids from the dietary fat. Follow-up experiments with different diets, especially high-carbohydrate diets, are needed to fully disentangle this.

We also found Ppar γ to be significantly upregulated in the liver of Pachón, Tinaja, and Molino cavefish compared to surface fish. Upon ligand activation, Pparγ induces many target genes involved in lipogenesis and adipogenesis, 21-25 making it a likely candidate transcription factor to explain the upregulation of some of the lipogenesis genes in cavefish. While Ppary has been shown to be upregulated in obese rodent models and human patients, 17,23,35,36 a role of Ppar γ in a species naturally adapted to food scarcity has, to our knowledge, not been reported before. Notably, we found the upregulation of $ppar\gamma$ to be already present in juvenile fish (before sexual maturation) and in specific response to the feeding event, further suggesting that it has an adaptive rather than pathological role. As Ppary plays important roles in adipogenesis, it is likely that the role of Ppary goes beyond the increased expression of lipogenesis genes but that Pparγ is also involved in increased adipogenesis in cavefish, potentially buffering the effect of lipotoxic lipid species.³⁷ Notably, we found evidence for increased genomic binding of Pparγ using ChIP-seg analysis. However, there are some limitations to this analysis. While we have validated the specifity of the antibody in vitro, we cannot fully exclude that some of the peaks are due to unspecific binding. We did identify a highly significant enrichment for the mouse Pparγ::Rxra motif in peaks near predicted transcription start sites; however, we do not know if the same motif is used in fish. Further functional analysis will be needed to fully disentangle this, but our analysis sets an important foundation for ChIP-seq analysis of transcription factors in non-traditional research systems.

Importantly, we identified additional signs of activation of Pparγ. We identified genomic mutations in one of its known repressors. Previous work has shown that Per2 represses Ppary directly and knockdown of Per2 leads to an increased activation of adipogenesis genes in vitro.30 These findings are in line with the observed phenotypes in the cavefish. While the per2 mutation is predicted to delete the Pparyy binding domain in Molino, in Pachón and Tinaja, the nonsense mutation is located 36 amino acids downstream of the predicted Pparyy binding domain, potentially leaving the binding domain intact (Figure 4D). While future experiments will be needed to explore whether these mutations affect protein structure, binding affinity for Ppar γ , or its ability to bind target regulatory elements, it is tempting to speculate that these mutations may attenuate the inhibitory effect of Per2 on Ppar γ -mediated transcription, which, in combination with higher levels of activators, would lead to higher transcriptional activity of Ppary.

Our finding of *per2* nonsense mutations in cavefish populations is interesting in terms of previous observations on this gene and circadian rhythms in general in cavefish. In studies of

circadian rhythm in *A. mexicanus*, it was found that the ability to entrain a circadian rhythm is not completely lost in cavefish but that there are differences in magnitude and timing of the rhythm.^{38,39} It has been speculated that this could be in part due to increased basal levels of *per2*.^{38,40} Our results add to these findings, potentially suggesting that Per2 is not fully functional even though its transcript is upregulated. However, it is clear that changes to circadian rhythm proteins are a hallmark of cavefish evolution. In this respect, it may be worth noting that icefish have also lost *per2*.⁴¹ This is further emphasized by the fact that we found mutations in *per2* in three independently derived cavefish populations, making *per2* a major target of evolution and highlighting important connections between circadian rhythm and metabolism.⁴²

STAR*METHODS

Detailed methods are provided in the online version of this paper and include the following:

- KEY RESOURCES TABLE
- RESOURCE AVAILABILITY
 - Lead contact
 - Materials availability
 - O Data and code availability
- EXPERIMENTAL MODEL AND SUBJECT DETAILS
 - Animals
- METHOD DETAILS
 - Body fat measurement
 - O Total lipid content quantification
 - Hepatic triglyceride measurement
 - H&E staining
 - Nile red staining
 - RNA-seq and transcriptome analysis
 - O RT-qPCR
 - Fatty acid profiling
 - Antibody generation
 - Western blot
 - HEK293T cell line overexpression
 - Immunofluorescence staining
 - ChIP-seq
 - Inhitibor treatment
 - Per2 genotyping
- QUANTIFICATION AND STATISTICAL ANALYSIS

SUPPLEMENTAL INFORMATION

Supplemental information can be found online at https://doi.org/10.1016/j.cub.2022.03.038.

ACKNOWLEDGMENTS

We thank Diana Baumann, Zachary Zakibe, Alba Aparicio Fernandez, Andrew Ingalls, David Jewell, Franchesca Hutton-Lau, Molly Miller, and Elizabeth Fritz for cavefish husbandry and support. We appreciate the support from Dai Tsuchiya, Seth Malloy, and Karen J. Smith of the Stowers histology support facility; the help from Rhonda Egidy, Amanda Lawlor, Michael Peterson, and Anoja Perera of the Stowers molecular biology support facility; the assistance from Alexis Murray, Olga Kenzior, and Chongbei Zhao of the Stowers tissue culture support facility; and the assistance of imaging analysis from Sean McKinney, Zulin Yu, Cindy Maddera, and Richard Alexander of the Stowers microscopy

Report



support facility. We thank the members of the Rohner lab for comments on the manuscript and four anonymous referees for review and critical suggestions. This work was done to fulfill, in part, requirements for S.X.'s PhD thesis research as a student registered with the Open University, U.K. This work was supported by institutional funding, NIH grant nos. 1DP2OD028806-01 and 1R01GM127872-01, and NSF EDGE award 1923372.

AUTHOR CONTRIBUTIONS

S.X. and N.R. conceived the project with additional contributions from W.W., A.K., L.O., J.K., J.P., K.M., R.P., Y.W., S.C., N.Z., N.T., J.M.M., and A.S.A. S.X., W.W., A.K., L.O., J.K., J.P., K.M., R.P., S.C., N.Z., and N.T. performed the research. S.X. and N.R. wrote the manuscript. All authors read and approved of the manuscript.

DECLARATION OF INTERESTS

The authors declare no competing interests.

Received: April 26, 2021 Revised: January 11, 2022 Accepted: March 11, 2022 Published: April 6, 2022

REFERENCES

- Kingsley, M.C.S., Nagy, J.A., and Russelll, R.H. (1983). Patterns of weight gain and loss for grizzly bears in northern Canada. Bears: Their Biology and Management 5, 174–178.
- Blem, C.R. (1976). Patterns of Lipid Storage and Utilization in Birds. Am. Zool. 16, 671–684.
- 3. Mitchell, R.W., Russell, W.H., and Elliott, W.R. (1977). Mexican eyeless characin fishes, genus Astyanax: environment, distribution, and evolution (Lubbock: Texas Tech Press).
- Aspiras, A.C., Rohner, N., Martineau, B., Borowsky, R.L., and Tabin, C.J. (2015). Melanocortin 4 receptor mutations contribute to the adaptation of cavefish to nutrient-poor conditions. Proc. Natl. Acad. Sci. USA 112, 9668–9673.
- Xiong, S., Krishnan, J., Peuß, R., and Rohner, N. (2018). Early adipogenesis contributes to excess fat accumulation in cave populations of Astyanax mexicanus. Dev. Biol. 441, 297–304.
- Hüppop, K. (2001). How do cave animals cope with food scarcity in caves?
 In Subterranean Ecosystems, H. Wilkens, D.C. Culver, and W.F. Humphreys, eds. (Amsterdam: Elsevier Press), pp. 417–432.
- Alié, A., Devos, L., Torres-Paz, J., Prunier, L., Boulet, F., Blin, M., Elipot, Y., and Retaux, S. (2018). Developmental evolution of the forebrain in cavefish, from natural variations in neuropeptides to behavior. eLife 7, e32808.
- Riddle, M.R., Boesmans, W., Caballero, O., Kazwiny, Y., and Tabin, C.J. (2018). Morphogenesis and motility of the Astyanax mexicanus gastrointestinal tract. Dev. Biol. 441, 285–296.
- Riddle, M.R., Aspiras, A.C., Gaudenz, K., Peuß, R., Sung, J.Y., Martineau, B., Peavey, M., Box, A.C., Tabin, J.A., McGaugh, S., et al. (2018). Insulin resistance in cavefish as an adaptation to a nutrient-limited environment. Nature 555, 647–651.
- Kersten, S. (2001). Mechanisms of nutritional and hormonal regulation of lipogenesis. EMBO Rep. 2, 282–286.
- Wang, Y., Viscarra, J., Kim, S.J., and Sul, H.S. (2015). Transcriptional regulation of hepatic lipogenesis. Nat. Rev. Mol. Cell Biol. 16, 678–689.
- 12. Numa, S., and Yamashita, S. (1974). Regulation of lipogenesis in animal tissues. Curr. Top. Cell. Regul. 8, 197–246.
- Folch, J., Lees, M., and Sloane Stanley, G.H. (1957). A simple method for the isolation and purification of total lipides from animal tissues. J. Biol. Chem. 226, 497–509.
- Medley, J.K., Persons, J., Peuss, R., Olsen, L., Xiong, S., and Rohner, N. (2020). Untargeted Metabolomics of the Cavefish Astyanax mexicanus

- Reveals the Basis of Metabolic Strategies in Adaptation to Extreme Conditions. Preprint at bioRxiv. https://doi.org/10.1101/2020.10.27. 358077.
- Ntambi, J.M., and Miyazaki, M. (2004). Regulation of stearoyl-CoA desaturases and role in metabolism. Prog. Lipid Res. 43, 91–104.
- Enoch, H.G., Catalá, A., and Strittmatter, P. (1976). Mechanism of rat liver microsomal stearyl-CoA desaturase. Studies of the substrate specificity, enzyme-substrate interactions, and the function of lipid. J. Biol. Chem. 251, 5095–5103.
- Yu, S., Matsusue, K., Kashireddy, P., Cao, W.Q., Yeldandi, V., Yeldandi, A.V., Rao, M.S., Gonzalez, F.J., and Reddy, J.K. (2003). Adipocyte-specific gene expression and adipogenic steatosis in the mouse liver due to peroxisome proliferator-activated receptor gamma1 (PPARgamma1) overexpression. J. Biol. Chem. 278, 498–505.
- Chong, M.F., Hodson, L., Bickerton, A.S., Roberts, R., Neville, M., Karpe, F., Frayn, K.N., and Fielding, B.A. (2008). Parallel activation of de novo lipogenesis and stearoyl-CoA desaturase activity after 3 d of high-carbohydrate feeding. Am. J. Clin. Nutr. 87, 817–823.
- Harding, S.V., Bateman, K.P., Kennedy, B.P., Rideout, T.C., and Jones, P.J. (2015). Desaturation index versus isotopically measured de novo lipogenesis as an indicator of acute systemic lipogenesis. BMC Res. Notes 8, 49.
- Klawitter, J., Bek, S., Zakaria, M., Zeng, C., Hornberger, A., Gilbert, R., Shokati, T., Klawitter, J., Christians, U., and Boernsen, K.O. (2014). Fatty acid desaturation index in human plasma: comparison of different analytical methodologies for the evaluation of diet effects. Anal. Bioanal. Chem. 406, 6399–6408.
- Ahmadian, M., Suh, J.M., Hah, N., Liddle, C., Atkins, A.R., Downes, M., and Evans, R.M. (2013). PPARγ signaling and metabolism: the good, the bad and the future. Nat. Med. 19, 557–566.
- Sharma, A.M., and Staels, B. (2007). Review: Peroxisome proliferator-activated receptor gamma and adipose tissue–understanding obesity-related changes in regulation of lipid and glucose metabolism. J. Clin. Endocrinol. Metab. 92, 386–395.
- 23. Lee, Y.J., Ko, E.H., Kim, J.E., Kim, E., Lee, H., Choi, H., Yu, J.H., Kim, H.J., Seong, J.K., Kim, K.S., and Kim, J.W. (2012). Nuclear receptor PPARγ-regulated monoacylglycerol O-acyltransferase 1 (MGAT1) expression is responsible for the lipid accumulation in diet-induced hepatic steatosis. Proc. Natl. Acad. Sci. USA 109, 13656–13661.
- 24. Tontonoz, P., and Spiegelman, B.M. (2008). Fat and beyond: the diverse biology of PPARgamma. Annu. Rev. Biochem. 77, 289–312.
- Schadinger, S.E., Bucher, N.L., Schreiber, B.M., and Farmer, S.R. (2005).
 PPARgamma2 regulates lipogenesis and lipid accumulation in steatotic hepatocytes. Am. J. Physiol. Endocrinol. Metab. 288, E1195–E1205.
- Feng, J., Han, J., Pearce, S.F., Silverstein, R.L., Gotto, A.M., Jr., Hajjar, D.P., and Nicholson, A.C. (2000). Induction of CD36 expression by oxidized LDL and IL-4 by a common signaling pathway dependent on protein kinase C and PPAR-gamma. J. Lipid Res. 41, 688–696.
- 27. Zhou, J., Febbraio, M., Wada, T., Zhai, Y., Kuruba, R., He, J., Lee, J.H., Khadem, S., Ren, S., Li, S., et al. (2008). Hepatic fatty acid transporter Cd36 is a common target of LXR, PXR, and PPARgamma in promoting steatosis. Gastroenterology 134, 556–567.
- Seargent, J.M., Yates, E.A., and Gill, J.H. (2004). GW9662, a potent antagonist of PPARgamma, inhibits growth of breast tumour cells and promotes the anticancer effects of the PPARgamma agonist rosiglitazone, independently of PPARgamma activation. Br. J. Pharmacol. 143, 933–937.
- Zizzo, G., and Cohen, P.L. (2015). The PPAR-γ antagonist GW9662 elicits differentiation of M2c-like cells and upregulation of the MerTK/Gas6 axis: a key role for PPAR-γ in human macrophage polarization. J. Inflamm. (Lond.) 12, 36
- Grimaldi, B., Bellet, M.M., Katada, S., Astarita, G., Hirayama, J., Amin, R.H., Granneman, J.G., Piomelli, D., Leff, T., and Sassone-Corsi, P. (2010). PER2 controls lipid metabolism by direct regulation of PPARγ. Cell Metab. 12, 509–520.



- 31. Herman, A., Brandvain, Y., Weagley, J., Jeffery, W.R., Keene, A.C., Kono, T.J.Y., Bilandžija, H., Borowsky, R., Espinasa, L., O'Quin, K., et al. (2018). The role of gene flow in rapid and repeated evolution of cave-related traits in Mexican tetra, Astyanax mexicanus. Mol. Ecol. 27, 4397-4416.
- 32. Ceinos, R.M., Frigato, E., Pagano, C., Fröhlich, N., Negrini, P., Cavallari, N., Vallone, D., Fuselli, S., Bertolucci, C., and Foulkes, N.S. (2018). Mutations in blind cavefish target the light-regulated circadian clock gene, period 2. Sci. Rep. 8, 8754.
- 33. Rinella, M.E. (2015). Nonalcoholic fatty liver disease: a systematic review. JAMA 313, 2263-2273.
- 34. Vernon, G., Baranova, A., and Younossi, Z.M. (2011). Systematic review: the epidemiology and natural history of non-alcoholic fatty liver disease and non-alcoholic steatohepatitis in adults. Aliment. Pharmacol. Ther. 34, 274–285.
- 35. Wolf Greenstein, A., Majumdar, N., Yang, P., Subbaiah, P.V., Kineman, R.D., and Cordoba-Chacon, J. (2017). Hepatocyte-specific, PPAR γ -regulated mechanisms to promote steatosis in adult mice. J. Endocrinol. 232, 107-121.
- 36. Pettinelli, P., and Videla, L.A. (2011). Up-regulation of PPAR-gamma mRNA expression in the liver of obese patients: an additional reinforcing lipogenic mechanism to SREBP-1c induction. J. Clin. Endocrinol. Metab. 96, 1424-1430.
- 37. Medina-Gomez, G., Gray, S.L., Yetukuri, L., Shimomura, K., Virtue, S., Campbell, M., Curtis, R.K., Jimenez-Linan, M., Blount, M., Yeo, G.S., et al. (2007). PPAR gamma 2 prevents lipotoxicity by controlling adipose tissue expandability and peripheral lipid metabolism. PLoS Genet. 3, e64.
- 38. Beale, A., Guibal, C., Tamai, T.K., Klotz, L., Cowen, S., Peyric, E., Reynoso, V.H., Yamamoto, Y., and Whitmore, D. (2013). Circadian rhythms in Mexican blind cavefish Astyanax mexicanus in the lab and in the field. Nat. Commun. 4, 2769.
- 39. Mack, K.L., Jaggard, J.B., Persons, J.L., Passow, C.N., Stanhope, B.A., Ferrufino, E., Tsuchiya, D., Smith, S.E., Slaughter, B.D., Kowalko, J., et al. (2020). Repeated evolution of circadian clock dysregulation in cavefish populations. PLoS Genet. 17, e1009642.
- 40. Frøland Steindal, I.A., Beale, A.D., Yamamoto, Y., and Whitmore, D. (2018). Development of the Astyanax mexicanus circadian clock and non-visual light responses. Dev. Biol. 441, 345-354.
- 41. Kim, B.M., Amores, A., Kang, S., Ahn, D.H., Kim, J.H., Kim, I.C., Lee, J.H., Lee, S.G., Lee, H., Lee, J., et al. (2019). Antarctic blackfin icefish genome reveals adaptations to extreme environments. Nat. Ecol. Evol. 3, 469-478.

- 42. Moran, D., Softley, R., and Warrant, E.J. (2014). Eyeless Mexican cavefish save energy by eliminating the circadian rhythm in metabolism. PLoS ONE
- 43. Kovner, I., Taicher, G.Z., and Mitchell, A.D. (2010). Calibration and validation of EchoMRITM whole body composition analysis based on chemical analysis of piglets, in comparison with the same for DXA. Int. J. Body Compos. Res. 8, 17-29.
- 44. Flynn, E.J., 3rd, Trent, C.M., and Rawls, J.F. (2009). Ontogeny and nutritional control of adipogenesis in zebrafish (Danio rerio). J. Lipid Res. 50, 1641-1652
- 45. Zhou, Y., Zhou, B., Pache, L., Chang, M., Khodabakhshi, A.H., Tanaseichuk, O., Benner, C., and Chanda, S.K. (2019). Metascape provides a biologist-oriented resource for the analysis of systems-level datasets. Nat. Commun. 10, 1523.
- 46. Schindelin, J., Arganda-Carreras, I., Frise, E., Kaynig, V., Longair, M., Pietzsch, T., Preibisch, S., Rueden, C., Saalfeld, S., Schmid, B., et al. (2012). Fiji: an open-source platform for biological-image analysis. Nat. Methods 9, 676-682.
- 47. Lawrence, M., Huber, W., Pagès, H., Aboyoun, P., Carlson, M., Gentleman, R., Morgan, M.T., and Carey, V.J. (2013). Software for computing and annotating genomic ranges. PLoS Comput. Biol. 9, e1003118.
- 48. Lawrence, M., Gentleman, R., and Carey, V. (2009). rtracklayer: an R package for interfacing with genome browsers. Bioinformatics 25, 1841-1842.
- 49. Zhang, Y., Liu, T., Meyer, C.A., Eeckhoute, J., Johnson, D.S., Bernstein, B.E., Nusbaum, C., Myers, R.M., Brown, M., Li, W., and Liu, X.S. (2008). Model-based analysis of ChIP-Seq (MACS). Genome Biol. 9, R137.
- 50. Yu, G., Wang, L.G., and He, Q.Y. (2015). ChIPseeker: an R/Bioconductor package for ChIP peak annotation, comparison and visualization. Bioinformatics 31, 2382-2383.
- 51. Yates, A.D., Achuthan, P., Akanni, W., Allen, J., Allen, J., Alvarez-Jarreta, J., Amode, M.R., Armean, I.M., Azov, A.G., Bennett, R., et al. (2020). Ensembl 2020. Nucleic Acids Res. 48 (D1), D682-D688.
- 52. Quinlan, A.R., and Hall, I.M. (2010). BEDTools: a flexible suite of utilities for comparing genomic features. Bioinformatics 26, 841-842.
- 53. Grant, C.E., Bailey, T.L., and Noble, W.S. (2011). FIMO: scanning for occurrences of a given motif. Bioinformatics 27, 1017-1018.
- 54. Fornes, O., Castro-Mondragon, J.A., Khan, A., van der Lee, R., Zhang, X., Richmond, P.A., Modi, B.P., Correard, S., Gheorghe, M., Baranašić, D., et al. (2020). JASPAR 2020: update of the open-access database of transcription factor binding profiles. Nucleic Acids Res. 48 (D1), D87-D92.



STAR***METHODS**

KEY RESOURCES TABLE

REAGENT or RESOURCE	SOURCE	IDENTIFIER
Antibodies		
Ppar _γ Antibody	GenScript	Custom made
Alexa Fluor® 568 goat anti-rabbit	Invitrogen	A-11011
anti-E-Cadherin	BD	610182
goat anti-rabbit	Invitrogen	A32733
donkey anti-mouse	Invitrogen	A31570
Chemicals, peptides, and recombinant proteins		
MS-222	Sigma	E10521
DNase	Promega	M6101
SYBR green	Quantabio	101414-288
DAPI	Sigma-Aldrich	D9542
TrueBlack® Lipofuscin Autofluorescence Quencher	Biotium	23007
Universal Blocking Reagent	BioGenex	HK085-5K
NEXTflex DNA barcodes	Perkin Elmer	NOVA-514104
DMSO	Corning	25-950-CQC
GW-9662	Enzy life sciences	BML-GR234-0050
Critical commercial assays		
Triglyceride Assay Kit	Abcam	ab65336
TruSeq Stranded mRNA Prep Kit	Illumina	20020594
Agencourt AMPure XP system	Beckman Coulter	A63881
high-capacity RNA-to-cDNA kit	applied biosystems	4387406
MicroBCA protein assay kit	Thermo Scientific	23235
MAGnify TM Chromatin Immunoprecipitation System	ThermoFisher	492024
KAPA HTP Library Prep Kit	Roche	KK8234
Deposited data		
Original data	Stowers Original Data Repository	https://www.stowers.org/research/publications/libpb-1619.
RNA-seq and ChIP seq data	GEO GSE173494	https://www.ncbi.nlm.nih.gov/geo/query/acc.cgi?acc=GSE173494
Code	Zenodo	https://doi.org/10.5281/zenodo.6080497.
Experimental models: Organisms/strains		
Surface, Pachon, Tinaja, and Molino populations of Astyanax mexicanus	Rohner lab	N/A
Oligonucleotides		
acaca_F 5'- CGCAGTGCCCATCTACGTG -3'	This paper	N/A
acaca_R 5'- TGTTTGGGTCGCAGACAGC -3'	This paper	N/A
aclya_F 5'- GGGCACCACAGTTTTTCCAA -3'	This paper	N/A
aclya_R 5'- CTGTCCGTGTGCCTGACTGA -3'	This paper	N/A
fasn_F 5'- GGGCACCACAGTTTTTCCAA -3'	This paper	N/A
fasn_R 5'- CTGTCCGTGTGCCTGACTGA -3'	This paper	N/A
rpl13a_F 5'- GTTGGCATCAACGGATTTGG -3'	This paper	N/A
rpl13a_R 5'- CCAGGTCAATGAAGGGGTCA -3'	This paper	N/A
pparγ_F 5'- GTCACCGCGATTCCTCTGAT-3'	This paper	N/A
pparγ_R 5'- ATCCCATGGGCCAGGAAAAC-3'	This paper	N/A
per2_F 5'- CGAGTTGTTTGGGGACCAAG-3'	This paper	N/A
		(Continued on payt page

(Continued on next page)





Continued		
REAGENT or RESOURCE	SOURCE	IDENTIFIER
per2_R 5'- ATCCATTCGAACCTGAGCCC-3'	This paper	N/A
Primers used to capture alternative splicing in Pachón and Tinaja (5'-3'): F: CATCACTGTGACGCTCTCATCATCCAG R: CTCAACCAGGGATGAACCTCAGCC	This paper	N/A
Primers used for Molino genomic DNA confirmation of 7 bp duplication (5'-3'): F: CTAGGCAGTAATGATCACCTGATGAG R: GACTTGCCTGGAGCCTTTCTGGTC	This paper	N/A
Software and algorithms		
RSEM	v1.3.0	https://deweylab.github.io/RSEM/
R	version 4.0.0	https://www.r-project.org
GenomicRanges	version 1.40	https://bioconductor.org/packages/release/bioc/html/ GenomicRanges.html
rtracklayer	version 1.48	https://bioconductor.org/packages/release/bioc/html/rtracklayer.html
MACS2	version 2.1.2	https://pypi.org/project/MACS2/
IDR	version 2.0.4.2	https://github.com/nboley/idr
ChIPseeker	version 1.24.0	https://bioconductor.org/packages/release/bioc/html/ChIPseeker.html
bedtools	version 2.29	https://bedtools.readthedocs.io/en/latest/
FIMO	version 5.3.0	https://meme-suite.org/meme/doc/fimo.html

RESOURCE AVAILABILITY

Lead contact

Further information and requests for resources and reagents should be directed to and will be fulfilled by the lead contact, Nicolas Rohner (nro@stowers.org).

Materials availability

Requests for the Ppary antibody should be made to Nicolas Rohner (nro@stowers.org) and will be fulfilled until the reagent expires.

Data and code availability

- Original data underlying this manuscript can be accessed from the Stowers Original Data Repository at https://www.stowers. org/research/publications/libpb-1619. RNA-seq and ChIP-seq data have been deposited at GEO and are publicly available under accession number GSE173494 at https://www.ncbi.nlm.nih.gov/geo/query/acc.cgi?acc=GSE173494.
- All original code has been deposited at Zenodo and is publicly available under https://doi.org/10.5281/zenodo.6080497.
- Any additional information required to reanalyze the data reported in this work paper is available from the lead contact upon request.

EXPERIMENTAL MODEL AND SUBJECT DETAILS

Animals

Surface, Tinaja, Pachón and Molino morphs of Astyanax mexicanus were reared at the Stowers Institute and all animal procedures were performed with IACUC approval. Those fish have been in a lab environment for nearly 20 years and roughly 6-8 generations away from wild caught fish. The aquatic animal program meets all federal regulations and has been fully accredited by AAALAC International since 2005. Astyanax were housed in polycarbonate tanks (~2 fish per liter), with a 14:10 h light:dark photoperiod. Each rack uses an independent recirculating aquaculture system with mechanical and biological filtration, and UV disinfection. Water quality parameters are maintained within safe limits (upper limit of total ammonia nitrogen range, 0.5 mg/L; upper limit of nitrite range, 0.5 mg/L; upper limit of nitrate range, 60 mg/L; temperature, 23°C; pH, 7.65; specific conductance, 800 μS/cm; dissolved oxygen, > 90% saturation). Standard water change rates range from 20% - 30% daily (supplemented with Instant Ocean Sea Salt [Blacksburg, VA]). A diet of Artemia nauplii (Brine Shrimp Direct, Ogden, Utah), Mysis shrimp (Hikari Sales USA, Inc., Hayward, CA), Gemma Micro, and Gemma Diamond 0.8 (Skretting USA, Tooele, UT) was fed to fry/juvenile/adult fish 4 - 12 months of age three



times daily at a designated amount and directly proportional to the density of fish within the tank. The nutritional composition of Gemma Micro, according to the manufacturer, is Protein 59%; Lipids 14%; Fiber 0.2%; Ash 13%; Phospohorus 2.0%; Calcium 1.5%; Sodium 0.7%; Vitamin A 23000 IU/kg; Vitamin D3 2800 IU/kg; Vitamin C 1000 mg/kg; Vitamin E 400 mg/kg. The nutritional composition of Gemma Diamond 0.8, according to the manufacturer, is Protein 57%; Lipids 15%; Fiber 0.2%; Ash 10.5%; Phospohorus 1.6%; Calcium 2.0%; Sodium 0.5%; Vitamin A 15000 IU/kg; Vitamin D3 2400 IU/kg; Vitamin C 1000 mg/kg; Vitamin E 250 mg/kg. The lipid profile of Gemma is the following: total fat as triglycerides: 12.87%; total monounsaturated fatty acids: 2.69%; total polyunsaturated fatty acids: 6.60%; total saturated fatty acids: 3.03%. Routine tankside health examinations of all fish were conducted by dedicated aquatics staff twice daily. *Astyanax* colonies are screened biannually for *Edwardsiella ictaluri*, *Mycobacterium* spp., *Myxidium streisingeri*, *Pseudocapillaria tomentosa*, *Pseudoloma neurophilia*, ectoparasites, and endoparasites using an indirect sentinel program.

METHOD DETAILS

Body fat measurement

The EchoMRI analyzer was used to quantify fish body composition. EchoMRI machine employs a nuclear magnetic resonance method for measuring the masses of fat, lean tissues, and water in tissues and organisms. ⁴³ Adult female fish (1 year old) with similar body sizes were euthanized with MS-222 and the ovaries were removed by dissection to avoid the effect of lipids in eggs on fat mass. The remaining carcasses were used for mass measurements. Replicates were measured and averaged as the readout for each sample. Fat mass normalized to total body weight was indicated as body fat content.

Total lipid content quantification

The Folch method 44 was used to measure total lipid content. In brief, we determined dry weight by drying tissue at 60° C for 48 h in 5 mL Eppendorf tubes (pre-weighted: W0), then measured the total weight of dried tissue and tube: W1, and calculated tissue dry weight: W1-W0. The whole tissue/organ was then homogenized with homogenizer (Benchmark Scientific, D1036) into powder. 1 mL chloroform: methanol = 2:1 (v/v) was added, then samples were washed with $200 \, \mu L 0.9\%$ NaCl. Homogenates were vortexed and centrifuged at $2,000 \, x$ g for 30 min. The lower layer (containing liquid) was transferred to pre-weighted aluminum weigh dishes (VWR, 25433-016). The liquid was dried in the hood completely (over 12 h). Then, the mass of the aluminum weigh dish containing lipids was determined using a Mettler Toledo (XS105 Dual range) balance. We calculated total lipid content of the tissue using following formula: Total lipid content = total lipids (mg) / tissue dry weight (mg) * 100%.

Hepatic triglyceride measurement

Fresh livers were collected and mass determined. Then the hepatic triglyceride was quantified using the Triglyceride Assay Kit (ab65336) according to the manufacturer's instructions. The triglyceride level was calculated using the following formula:

Hepatic triglyceride measurement = triglyceride (μg) / fresh liver weight (mg) *100%.

H&E staining

The fish head and trunk were dissected and fixed in 4% paraformaldehyde for 18 h at 4 $^{\circ}$ C and embedded in paraffin while following kit instructions for dehydration, infiltration and embedding. Tissues were sectioned at 10 μ m and slides were dried for 1 h in a 60 $^{\circ}$ C oven. Then, slides were stained with hematoxylin for 3 min and eosin for 1 min. Slides were washed with desalted water and air-dried. Images were obtained using a VS120 virtual slide microscope (Olympus) and analyzed with ImageJ. We used \sim 1 year old female fish of similar sizes for this experiment.

Nile red staining

For adult fish head Nile red staining: the fish heads were dissected and washed in PBS three times to remove residual blood. Then heads were immersed in 1 μ g/mL Nile red working solution at 4 degree for 7 days. The stained samples were washed with PBS and used for imaging. For fish larvae Nile red staining: the fish larvae were washed with PBS and immersed in 1 μ g/mL Nile red working solution at room temperature for 30 min. The stained larvae were washed with PBS and euthanized with 500 mg/L MS-222 before imaging. Images were obtained using a M205 C (Leica) microscope with an DFC7000 T (Leica) camera under GFP channel and analyzed with ImageJ. Shortly, wand tool in ImageJ was used to define the edge of adipose tissue and the area was measured using "Measure" under the "Analyze" menu.

RNA-seq and transcriptome analysis

We used 4 months old fish for this experiment because at this stage the livers are big enough to be dissected for RNA harvest and the fish are not sexually mature, which can affect lipid metabolism heavily. Fish were housed individually for the experiment. Each fish was fed 10 mg Gemma twice per day for at least one week to allow the fish acclimate to the new environment. (Various amounts of Gemma were fed to test their effect on lipogenesis in the liver, we found 10 mg Gemma can stimulate lipogenesis to different levels while not saturate the gene expression levels.) Once the fish were used to the new feeding regime, they were all fasted after one feeding (10 mg Gemma per fish) for 4 days. These fish were termed as the fasted group. Half of the fish (3 surface and 3 Pachón cavefish) were refed 10mg Gemma after 4 days fasting and were termed the refed group. 3 h after feeding, fish liver samples





were dissected quickly, rinsed with cold PBS, and snap-frozen in liquid nitrogen. We chose 3 h after feeding as the best time point due to preliminary time course experiments. Total RNA was extracted using Trizol reagent (Ambion). Libraries were prepared according to manufacturer's instructions using the TruSeq Stranded mRNA Prep Kit (Illumina). The resulting libraries were purified using the Agencourt AMPure XP system (Beckman Coulter) then quantified using a Bioanalyzer (Agilent Technologies) and a Qubit fluorometer (Life Technologies). Libraries were re-quantified, normalized, pooled and sequenced on an Illumina HiSeq 2500 using v4 High Output chemistry, single read 50bp, RTA v1.18.64, and bcl2fastq2 v2.20 for demultiplexing and FASTQ file generation. Both surface fish and Pachón cavefish reads were aligned to surface fish genome (Astyanax_mexicanus-2.0) via STAR aligner (v2.6.1c), under Ensembl 91 gene model. TPM gene expression values were generated using RSEM (v1.3.0). Pairwise differential expression analysis was performed using R package edgeR for different fish under different conditions. GO term enrichments were done based on upregulated and downregulated DE genes using Metascape. 45

RT-qPCR

The cDNA was made from 1 ug total RNA (from previous step) with high-capacity RNA-to-cDNA kit (applied biosystems, 4387406) and treated with DNase. (Promega, M6101) qPCR was conducted on a QuantStudio 6 Flex Real-Time PCR System with SYBR green detection. (Quantabio, 101414-288)). Amplification specificity for each real-time PCR reaction was confirmed by analysis of the dissociation curves. Determined C_t values were then exploited for further analysis, with the rpl13a gene as the reference. Each sample measurement was made in triplicate. Primer sequences for acaca were acaca_F 5'- CGCAGTGCCCATCTACGTG -3' and acaca_R 5'-TGTTTGGGTCGCAGACAGC -3'. For aclya, the primer sequences were aclya_F 5'-GGGCACCACAGTTTTTCCAA -3' and aclya_R 5'- CTGTCCGTGTGCCTGACTGA -3'. For fasn, the primer sequences were fasn_F 5'- GGGCACCACAGTTTTTCCAA -3' and fasn R 5'- CTGTCCGTGTGCCTGACTGA -3'. For rpl13a, primers were rpl13a F 5'- GTTGGCATCAACGGATTTGG -3' and rpl13a_R 5'- CCAGGTCAATGAAGGGGTCA -3'.

For ppary, primers were ppary_F 5'- GTCACCGCGATTCCTCTGAT-3' and ppary_R 5'- ATCCCATGGGCCAGGAAAAC-3'. For per2, primers were per2_F 5'- CGAGTTGTTTGGGGACCAAG-3' and per2_R 5'- ATCCATTCGAACCTGAGCCC-3'.

Fatty acid profiling

The fatty acid profiling data were extracted from.²¹ In brief: A group of 6 surface and 6 Pachón were starved for 30 days before dissected for liver collection (30d_fasted). A second group of 6 surface and 6 Pachón were fed regulary until 4 days before dissection (4d_fasted). A third group of 6 surface and 6 Pachón were fed regulary until 4 days before dissection. Then, on the day for dissection, they were refed 10 mg Gemma 500. Then 3 h after they were refed, livers were collected (refed). All the livers were snap frozen and shipped to West Coast Metabolomics Center on dry ice. Fatty acids abundances were determined by charged-surface hybrid column-electrospray ionization quadrupole time-of-flight tandem mass spectrometry (CSH-ESI QTOF MS/MS). Data was reported as peak height using the unique quantification ion at the specific retention index.

Antibody generation

The protein sequence of Ppar_Υ was used to blast against Astyanax genomes (Astyanax_mexicanus-1.0.2 and Astyanax_mexicanus-2.0) to evaluate similarity of Ppar γ to other proteins in the genome. We chose 227-564aa of Ppar γ as antigen for its relatively high specifity. This 338aa protein fragment was then expressed in E.coli and used to immunize two rabbits for antibody production by GenScript. ELISA titer > 1:128,000 and target protein fragment binding validation were done by western blot and cell line overexpression.

Western blot

For western blot, we used four-months-old juvenile fish. The feeding regime was the same as those fish for RNA-seq. Fish liver samples were dissected quickly, rinsed with cold PBS, and snap-frozen in liquid nitrogen. Western blotting was performed using standard protocols. Briefly, liver tissues were lysed in RIPA buffer and total protein concentrations were determined by MicroBCA protein assay kit (Thermo Scientific, 23235) according to the manufacturer's instructions and infinite 200 PRO microplate reader (Tecan). For each sample, 10 µg total protein were loaded to each well to run SDS-PAGE gel, protein transfer from gel to pvdf membrane, blocking, and antibody incubation. Imaging was carried out with Odyssey CLx system (LI-COR). The band intensity was calculated with FIJI. In short, "Rectangular" was used to include the each protein band in the image, then plot was made using "Plot lanes" under "Gels" in the "Analyze" menu. "Straight" was used to define the bottone line and area was measured using "Measure" under the "Analyze" menu.

HEK293T cell line overexpression

The surface fish and Pachón cavefish $ppar\gamma$ coding regions were cloned from cDNA, then they were inserted into pDestTol2 vector under the control of the hsp70 promoter (from zebrafish). 7.5 μL FuGene (E2311) and 2.5 μg plasmid were transfected into HEK293T cells on glass bottom microwell plates (MetTek, P35G-1.5-14-C). 24 h later, 41°C heat shock for 1 h was performed. 48 h after transfection, cells were fixed with 4% pfa for 20 min at room temperature (RT). Cells were permeabilized with PBST (0.1% Triton X-100) for 30 min at RT. Blocking was performed with Universal Blocking Reagent (BioGenex, HK085-5K,) for 1 h at RT. A series of anti-Pparγ antibody dilutions were used to incubate cells for 2 h at RT. After PBST (0.1% Triton X-100) wash, cells were incubated with Alexa Fluor® 568 goat anti-rabbit (Invitrogen, A-11011) and DAPI (Sigma-Aldrich, D9542) for 1 h at RT. After PBS wash, cells were imaged with Axiovert 200M microscope.



Immunofluorescence staining

Liver tissues were fixed with 4% pfa for 16 hous at 4°C. Then liver sections (10 µm) were done through cryostat sectioning. Slides were treated with PBS to get rid of OTC and permeabilized with 0.1% PBST (Triton X-100) for 45 min. Blocking was performed at room temperature for 1 h. Samples were treated with TrueBlack® Lipofuscin Autofluorescence Quencher (Biotium, 23007) before addition of primary antibody. Then, Primary antibody incubation was carried out at 4°C overnight. Secondary antibody and DAPI (Sigma-Aldrich, D9542) incubation were done at room temperature for 3 h. The antibodies in this study include anti-Pparγ (see antibody generation), anti-E-Cadherin (BD Transduction Laboratories, 610182), goat anti-rabbit (Invitrogen, A32733), and donkey antimouse (Invitrogen, A31570). Images were taken with Leica TCS SP8 X microscope and analyzed with ImageJ. In short, nuclei were segmented using a Log3D and Fiji's 3D MaximumLocal finder to find nuclear centroids, and the 3D Spot Segmentation plugin to separate objects. Once objects were found, background subtraction was performed and mean channel intensities were found per blob. These were averaged over the whole image and plotted as shown. For E-cadherin and Pparγ channel, intensities were measured similarly.46

ChIP-seq

Livers from eight juvenile fish (four-month-old) were pooled together and snap frozen. Then the frozen tissues were ground into powder, followed by 1% pfa (diluted from 16% pfa, Thermo Fisher, Pl28906) fixation for 10 min at room temperature. The cross link was quenched with 0.125 M glycine. Chromatin shearing was performed by using a Bioruptor sonication system with following parameters: 30 s on and 30 s off per cycle, 10 cycles in total. DNA fragments were collected and purified with MAGnify Chromatin Immunoprecipitation System (ThermoFisher, 492024) according the kit instruction. Purified DNA (~10 ng) for each sample was taken as input to construct the library. Libraries were prepared using the KAPA HTP Library Prep Kit (Roche, KK8234) with 15 cycles of PCR and using 1:125 dilution of NEXTflex DNA barcodes (Perkin Elmer, NOVA-514104). The resulting libraries were purified using the Agencourt AMPure XP system (Beckman Coulter) then quantified using a Bioanalyzer (Agilent Technologies) and a Qubit fluorometer (Life Technologies). Post amplification size selection was performed on all libraries using a PippinHT (Sage Science). High throughput sequencing was performed on the Illumina NextSeq platform. Both surface fish and Pachón cavefish reads were aligned to surface fish genome (Astyanax mexicanus-2.0). Genome browser track files in bigWig format were generated using R (version 4.0.0) packages GenomicRanges (version 1.40)⁴⁷ and rtracklayer (version 1.48).⁴⁸ Signals were normalized to fragments/reads per million (RPM). Peaks were called using MACS2 (version 2.1.2)⁴⁹ for individual and merged replicates (q-value cutoff of 0.01). Next, IDR (https://github.com/nboley/idr, version 2.0.4.2) was used to keep those peaks that occurred consistently in both replicates. We further filtered peaks using fold enrichment and q-value cutoffs at summit position (fold enrichment 3 5 and q-value £ 1E-20). We took the summit position of the filtered peaks and used R package ChIPseeker (version 1.24.0)⁵⁰ to annotate the peaks to genomic scription end site), and distal intergenic regions. Astyanax genome annotation was obtained from Ensembl 98.51 We combined and merged filtered peaks for Pachón and surface using bedtools (version 2.29). 52 For each merged peak, the new summit was assigned as the median of all overlapping peaks. Then the merged peaks were resized to 401 bp by extending 200 bp upstream and downstream of the new summits. The resized peaks were treated as the meta-peak list. We used FIMO (version 5.3.0)⁵³ to scan the occurrences (p value cutoff of 1E-5) of mouse Pparyg motifs (MA0065.2 in JASPAR 2020 database⁵⁴ in 10351 meta-peaks falling into promoter regions (defined as ± 3 Kb from transcription start site). To test motif enrichment, we randomly placed these meta-peaks in the promoter regions of all protein coding genes and performed FIMO scan using the same parameters. This shuffle process was repeated 1000 times.

Inhitibor treatment

The 5dpf fish larvae of surface fish and Pachón cavefish were placed in a plastic cup with a mesh on the bottom (hole size = 200 µm), then the cup with fish was placed in a 3L tank. Fish larvae were fed with 40 mg Artemia twice per day (morning feeding and afternoon feeding) from 5dpf to 10dpf. After the afternoon feeding, the fish larvae were treated with 0.2% DMSO (Corning, 25-950-CQC) or 40 μM GW-9662 (Enzy life sciences, BML-GR234-0050) for 3 h each day. Different concentrations of the inhibitor were tested and 40 μM was deemed high enough to inhibit lipid accumulation in both fish populations. Then the fish larvae were transferred back to 3L tanks containing fresh fish water. At 11dpf, the larvae were only fed in the morning, after which we collected the larvae, performed Nile red staining, euthanized and imaged the larvae.

Per2 genotyping

Primers used to capture alternative splicing in Pachón and Tinaja (5'-3'):

Forward: CATCACTGTGACGCTCTCTCATCATCCAG Reverse: CTCAACCAGGGATGAACCTCAGCC

PCR conditions: Denaturing 95°C 30 s - Annealing 57°C 30 s - Extension 72°C 45 s 35 cycles

Primers used for Molino genomic DNA confirmation of 7 bp duplication (5'-3'):

Forward: CTAGGCAGTAATGATCACCTGATGAG Reverse: GACTTGCCTGGAGCCTTTCTGGTC

PCR conditions: Denaturing 95°C 30 s - Annealing 56°C 30 s - Extension 72°C 60 s 35 cycles





QUANTIFICATION AND STATISTICAL ANALYSIS

We used R to do statistical analysis, except for the RNA-seq data differential expression analysis where we used EdgeR. All numbers of animals or cells used for the experiments and the statistical test method used can be found in the corresponding figure legends. Generally, we assigned the significance level based on p value in following manner: *p < 0.05; **p < 0.01, ****p < 0.001, ****p < 0.001.